Photocatalytic nanocomposite anatase–rutile TiO2 coating

Fatemehsadat Moosavi, Alex Lemarchand, Cyrille Bazin, Maria Konstantakopoulou, Mathieu Frégnaux, Christophe Colbeau-Justin, Touraj Tavakoli Gheinani, Andrei Kanaev, Mehrdad Nikravech

Photocatalytic nanocomposite anatase-rutile TiO_2 coating

Fatemehsadat Moosavi[1], Alex Lemarchand[1], Cyrille Bazin[2], Maria Konstantakopoulou[1], Mathieu Frégnaux[3], Christophe Colbeau-Justin[4], Touraj Tavakoli Gheinani[5], Andrei Kanaev[1*], Mehrdad Nikravech[1]

[1] *Laboratoire des Sciences des Procédés et des Matériaux, CNRS, Université Sorbonne Paris Nord, 93430 Villetaneuse, France*
[2] *Laboratoire Interfaces et Systèmes Electrochimiques, Sorbonne Université, 75252 Paris cedex 05, France*
[3] *Institut Lavoisier de Versailles, UMR 8180, CNRS, UVSQ - Université Paris-Saclay, 78035 Versailles cedex, France*
[4] *Institut de Chimie Physique, CNRS UMR 8000, Université Paris-Saclay, 91405 Orsay, France*
[5] *Department of Chemical Engineering, Faculty of Engineering, University of Isfahan, Isfahan, Iran*

Received ZZZ, revised ZZZ, accepted ZZZ
Published online ZZZ (Dates will be provided by the publisher.)

Keywords: nanocomposite TiO_2 coating, anatase, rutile, adherence, photocatalysis.
* Corresponding author: andrei.kanaev@lspm.cnrs.fr; Phone: +33 1 49 40 34 30; Fax: +33 1 49 40 34 14

Nanocomposite TiO_2 coatings of mixed anatase-rutile crystalline polymorphs with strong adherence to glass substrates were prepared via spray-plasma deposition method. The rutile content was varied between 0 and 30 mol%. The coating showed an enhanced photocatalytic activity towards cefixime antibiotic decomposition in aqueous solutions under UVA (λ=365 nm) light illumination. The activity significantly increased after the rutile phase formation, suggesting a synergetic effect of the two-component solids.

1. Introduction

Titanium dioxide (TiO_2) has deserved large interest in photocatalysis, becoming nowadays a key material in the environmental protection [1-3]. However, studies of its optimal composition under UV and sun illuminations still continue. Advances in preparation methods of photcatalytic titania coatings have been recently reviewed [4]. Between different polymorphs, anatase TiO_2 with the bandgap of 3.2 eV generally showed a higher activity and rutile TiO_2 with the bandgap energy of 3.0 eV possesses a lower activity, which has been mainly related to the radicals generation at respective (101) and (110) thermodynamically stable crystalline facets [5-7]. Attempts to increase of the adsorption capacity of rutile TiO_2 have been undertaken, conducting to a significant enhancement of the photocatalytic activity [8]. In the same time, one of the best photocatalytic performances showed a commercial composite TiO_2, Degussa P25, which up to now is considered as the reference photocatalytic material. This material appeared in a powder form, composed of agglomerated nanoparticles of 15-30 nm size of mixed anatase (~70 %) and rutile (~30 %) polymorphs with a small addition of an amorphous material [9, 10]. Previous studies [11, 12] have revealed a significant inhibition of the electron-hole recombination process in this material, which has a consequence of the photocatalytic activity enhancement [13-15]. It has been also suggested that small particles of size ~10 nm possess a higher activity compared to larger particles [16-18], which corresponds to Degussa P25 TiO_2 nanopowders.

Despite of much progress in understanding of the functional properties, large scale applications of this composite-phase photocatalyst is rather limited because of the severe problems related to environmental pollution by photocatalytic nanoparticles. The filtering of effluents via filtration from suspended nanoparticles in a liquid phase is generally expensive and of insufficient effectiveness. Furthermore, a tendency of semiconducting nanoparticles to aggregation decrease both light coupling efficiency and charge transfer efficiency to active surface sites, which finally worsen their functional response. The depositions of Degussa P25 TiO_2 nanopowders on appropriate supports, though being successful [19], have not resulted in mechanically strong coatings. Therefore, elaboration of photocatalytic nanocoatings with the structural composition equivalent to that of Degussa P25 remains a challenging task.

In this work we developed a preparation method of photocatalytically active coatings with crystalline grain size ~10 nm and unique anatase-rutile phase composition, which can be adjusted. These coatings were mechanically stable, forming strong covalent bonds with supports, which

permits considering them for large-scale applications in the environmental photocatalysis.

2. Experimental

The TiO_2 films were deposited on glass beads by using the low-pressure spray plasma method [20, 21]. Before operation, the reaction chamber was maintained under vacuum of 20 Pa by a continuous pumping. Microscopic droplets of about 0.5 μm size of a titanium tetra isopropoxide (Sigma-Aldrich) solution in 2-propanol (Sigma-Aldrich) with volume ratio 1:1 were produced by an ultrasonic nebulizer Mist Maker DK24 (ServoVendi) operating at 1 MHz frequency and injected into the reaction chamber via argon carrier gas at a flow rate of 300 ml/min. A special aerosol conditioner was used to introduce aerosol from atmospheric pressure into the low pressure plasma reactor. The oxygen gas as a reactive component was admixed to the argon gas flow at a rate varying between 0 and 25 ml/min. A plasma discharge was initiated in the reaction chamber by using an inductive radiofrequency generator (Hüttinger Trumpf Qinto 3013, 3 kW, 13.5 MHz) of 300 W power. The glass beads, preliminarily cleaned in sulfuric acid and distilled water, were positioned in a fixed bed inside the plasma reactor chamber and the deposition time was fixed to 60 min. In order to improve the crystallinity, the coatings were post-treated thermally in a furnace RHTC-80230115 (Nobertherm) at 450 °C during 4 hours.

The x-ray diffraction (XRD) patterns were collected at a grazing incidence using Panalytical Empyrean diffractometer equipped with Cu-Kα source (λ=1.541 Å). The x-ray incident beam was collimated with 1/16° slits coupled with a 5 mm mask to ensure that the beam footprint did not exceed the sample surface. The diffractometer was equipped with PIXcel1D 255-channels detector operating in scanning line mode coupled with a parallel plate collimator (acceptance angle of 0.18°). The patterns were collected with an incident angle of 0.5° in the range from 15° to 70° (2θ) with a step of 0.03° and counting time per step of 75 s. The phase quantification was estimated from the Grazing Incidence XRD (GIXRD) patterns with rutile/anatase ratio calculated from the respective (110) and (101) peak intensities via equation $F_r=1-(1+1.265\cdot I_{r110}/I_{a101})^{-1}$ [22]. The high-resolution transmission electron microscopy (HRTEM) was performed using JEOL 2011 equipment operating at 200 kV with LaB_6 electron emission source. The images were recorded using Gatan MultiScan CCD camera positioned at the output of Gatan Imaging Filter system. Samples were prepared by tearing off some pieces of the thin film and depositing on holey carbon film supported 400 mesh copper grids. The interplanar lattice spacing of TEM patterns was analyzed with ImageJ 1.53k software [23]. The XPS analysis was realized on Thermofisher Scientific Escalab 250xi equipment with spot size of 650 μm and flood gun assistance (Al-Kα, λ=1486.6 eV, Pass Energy (survey/HR) 100 eV / 20 eV, dwell time 100 ms, step (survey/HR) 1 eV / 0.1 eV). Spectra were then charge corrected by shifting all peaks to the adventitious C1s spectral component (C-C, C-H) binding energy set to 284.8 eV. Quantification is performed based on the photopeak areas after a Shirley type background subtraction using the Thermofisher Scientific Avantage© software and its "ALTHERMO1" library as sensitivity factor collection.

The time-resolved microwave conductivity (TRMC) measurements providing lifetime of photoinduced charges were realised at the experimental installation described in Ref. [24]. The method is based on a variation of the microwave power reflected by a semiconductor irradiated with a pulsed laser, inducing changes of the electrical conductivity. The samples were irradiated with 360-nm light pulses of 8 ns duration and 1.3 mJ energy delivered by cw OPO Nd:Yag laser (EKSPLA) operating at 10 Hz. The irradiated area on a sample was 5 mm in diameter. The measurements were conducted at room temperature under ambient atmosphere. The recorded signal was accumulated over 200 laser pulses.

The photocatalytic activity of the prepared materials was evaluated by the degradation of cefixime antibiotic in aqueous solutions under UV-lamp illumination in a continuous-flow fixed-bed reactor described in Ref. [25]. In brief, 10 mg/l cefixime solution in distilled water was placed in a reservoir and pushed by a peristaltic pump into the 6-mm gap between two coaxial quartz reactor tubes, filled with 100 g of the coated glass beads of 3-mm diameter, forming a packing bed of about 6 cm height. The light source, UVA lamp Phillips TL BLB with 8 W power emitting at 365 nm with full-width at half maximum $\Delta\lambda_{1/2}$=16 nm, of a cylindrical geometry was inset in the inner reactor tube maintained at 25 °C by circulating the gas flow through a heat exchanger. The pollutant concentration was periodically measured by absorption at 286 nm, using a compact optical fiber coupled PC-plugged AvaSpec-Mini UV/VIS/NIR Spectrometer (spectral resolution of 0.5 nm). Before illumination, the pollutant flow was passed through the reaction medium during 4 hours in order to attain the adsorption-desorption equilibrium of the pollutant molecules on the photocatalyst. Then the UVA lamp was set "on" and the pollutant concentration measurements were continued under illumination. Blank tests were realized in the empty reactor in order to evaluate the photolytic decomposition of pollutant by lamp photons. The reproducibility of the experimental series was verified. We notice that the applied monitoring degradation kinetic was used to evaluate the photocatalyst activity and does not indicate that cefixime molecules were totally oxidized into small inorganic species such as H_2O, CO_2, etc., which can be inferred using Total Organci Carbon (TOC) analysis. The intermediate cefixime oxidation products can persist in our

case after the irradiation period. Such intermediate products of cefixime photodegradation have been recently reported [26].

3. Results and discussion

Table 1 summarizes the preparation conditions and resulting crystalline composition of the prepared coatings. The respective structural data were obtained from the analysis of GIXRD patterns, some of which are shown in Fig. 1.

Table 1: Oxygen gas flow conditions and crystalline composition of coatings.

coating	oxygen gas flow (mL/min)	anatase crystalline size (nm)	rutile crystalline size (nm)	rutile content [(1)] (mol%)
D1	0	9.3	-	0
D2	2	9.6	8.1	16
D3	10	8.7	8.5	27
D4	25	8.5	8.1	30

[(1)] Complementary to anatase phase

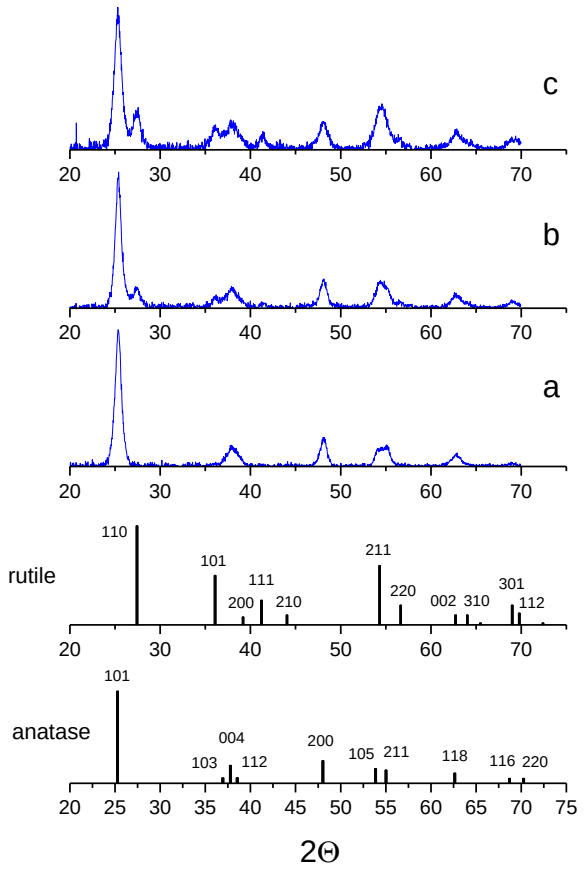

Figure 1: X-ray diffraction patterns (Cu-Kα radiation source) of TiO_2 coatings D1 (a), D2 (b) and D3 (c). Peaks positions of anatase (COD – ID 9015929) and rutile (COD – ID 9015662) TiO_2 polymorphs [27] are indicated below.

The oxygen gas flow in the plasma appeared to be one of key factors in the elaboration of composite anatase-rutile TiO_2 coatings. Indeed, in the absence of oxygen almost pure anatase phase was observed in sample D1 (Fig. 1c), while an increase of the oxygen flow resulted in a strong increase of the rutile content up to 16 mol% in sample D2 (Fig. 1b) and 27 mol% in samples D3 (Fig. 1c). At even higher doubled oxygen content, the rutile phase insignificantly increased to ~30 mol%. The characteristic size of the crystalline domains, of both anatase and rutile polymorphs, determined by Scherrer relation was very similar of 9±1 nm.

The HRTEM images confirm these results, showing well crystallised materials with the mean grain size about 10 nm: anatase and rutile domains coexist in the appropriate samples (example of D4 is shown in Fig. 2). The appearance of rutile phase after heat treatment at 450 °C was unexpected. In fact, previous studies have shown that rutile appeared in single TiO_2 nanoparticles of size larger than 14 nm [28, 29] and in agglomerated nanopowders at temperatures above 550 °C (with the heat treatment duration of 4 h) [29, 30]. The rutile phase appearance is suggested to occur through the interface nucleation at a contact area between two anatase nanoparticles in a particular orientation [31]. More favourably, it is initiated at the twin (112) anatase interface, which involves structural elements common to rutile [32]; this transformation requires lower activation energy compared to that at the surface or in the bulk.

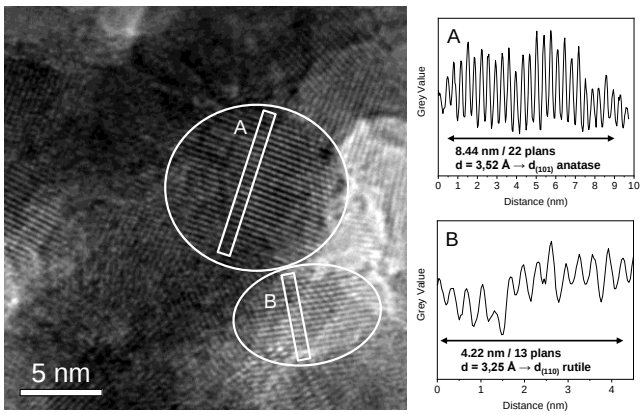

Figure 2: HRTEM image of D4 coating (left) and analysis of interplane distances of anatase and rutile lattices (right).

On the other hand, the mixed anatase and rutile phase composition has been reported in films deposited with pulsed micro-plasma cluster source [33]. A variation of the stoichiometry has been disregarded in these experiments because of the strictly homogeneous elemental condition O:Ti=2:1. As a result, these authors have suggested that the structure of the very small titania clusters is predisposed for the rutile formation while that of larger particles (of size above 5 nm) converges to anatase crystallites. A control of the crystalline anatase/rutile composition could be therefore

achieved via selection of cluster during the deposition process.

Despite of the oxygen gas insertion in the plasma chamber, its impact on the films stoichiometry can be neglected in our experiments. Indeed, the XPS elemental analysis of the film composition of D1 and D3 samples resulted in the same ratio of O/Ti=1.97, which can be considered as stoichiometric. Most probably, and in agreement with earlier studies [33, 34], the oxygen content affects the size and surface state of the condensed species coming from plasma and impinging substrates. The influence of plasma oxygen on physicochemical properties of oxide coatings has been previously reported [21, 35]. The polydispersity and/or inhomogeneity of the condensed species controlled by the oxygen content apparently define the anatase/rutile ratio of prepared films.

An interesting observation is however the formation of similar sizes of anatase and rutile crystallites evidenced by GIXRD and TEM data. This makes doubtful the proposed cluster size effect on TiO_2 polymorph formation [33], since smaller clusters and bigger nanoparticles are not expected to result in the same size entities after crystallisation. We believe that the surface state is responsible for the rutile phase appearance. In fact, the standard free energy change is expressed by

$$\Delta G^0=\Delta_f G^0(T)_2-\Delta_f G^0(T)_1+A_2\gamma_2-A_1\gamma_1 \qquad (1)$$

where $\Delta_f G^0$ is the standard free energy of two phases formation and A and γ are respectively surface area and surface free energy of the particles. The condition of $\Delta G^0=0$ enables the phase transformation $1\rightarrow2$ (anatase$\rightarrow$rutile) and it obviously depends on the surface state and size of a particle and temperature T [28].

Low pressure plasmas, under which the layers were elaborated, are known as thermodynamically non-equilibrium media. It is noteworthy that in these conditions oxygen molecules undergo dissociative reactions leading to generation of reactive oxygen radicals [20, 34]. The exothermic recombination reactions, particularly those of oxygen radicals on the surface of deposit, could also enhance local temperature leading to the rutile phase formation on some sites while the surroundings remain cold. More oxygen radicals are produced in plasma, more recombination reactions take place and, consequently, more rutile crystallites could be produced, in accordance with the correlation between rutile contents and oxygen gas flow observed in our experiment (Table 1).

The Ti2p, O1s and Si2p XPS spectra of coatings, one example of which is given in Fig. 3, were quite similar. The crystalline composition of the prepared coatings is summarized in Table 1. The Ti2p core level peaks (23.3 at.%) with binding energies of 458.9 eV ($2p_{3/2}$) and 464.6 eV ($2p_{1/2}$) and the satellite peak related to surface plasmon at 472.2 eV are characteristic of Ti^{4+} cation in TiO_2 [36]. No significant signal of partially reduced Ti^{n+} (n<4) to the lower energies from the principal Ti2p peaks [37] have been observed in our spectra, which confirms stoichiometry of the produced TiO_2 films. However, a weak $Ti2p_{3/2}$ contribution suggests a minor (~2 at.%) appearance of suboxide Ti^{3+} at 457.4 eV, which nature will be discussed below. The O1s spectra were de-convoluted into three peaks at 530.2 eV (46.3 at.%) 531.2 eV (3.4 at%) and 532 eV (8.9 at.%). The lower energy one originates from Ti–O–Ti bonds, while the less intense one at higher binding energy was attributed to the physisorbed species (O_{phs}), typically oxidised carbonaceous species, supported by observation of four C1s contributions in the vicinity of 285 eV with the total content of 15.5 at% (not shown). The O1s intermediate energy chemical environment could belong to O in cross-linking bonding Ti–O–Si [36, 38, 39]. We notice that a weak peak associated with Si–O–Si bonds at about 533.0 eV could not be identified in the intense spectrum of O1s because of the screening of pure silica substrate by TiO_2 coating. This O1s analysis might indicate (O)3≡Ti–O–Si≡(O)3 bonds formed between the coating and substrate. However, Ti-O-H bonds [36] could also contribute at this energy that may compromise the assignment. The Si2p spectra were therefore recorded to verify this point.

The Si2p spectrum in Fig. 3 with the maximum at 102.3 eV and full-width at half maximum $\Delta E_{1/2}$=1.8 eV (Fig. 3) can be due to Si^{3+} suboxide [40, 41], which chemical shift of 1.05 eV per oxidation state of Si^{n+} has been earlier established [42]. Its intensity was significantly weaker compared with Ti2p and O1s spectra, owing to the screening effect of the TiO_2 film. Surprisingly, the signal of Si^{4+} at 103.8 eV characteristic of silica was missing, which is expected to come from silica substrate. We notice in this respect that the peak at ~102-103 eV is a common feature of silicon exposed to plasmas and according to Cardinaud et al. [43] could only be indicative of the Si^{n+} oxidation state and belong to an ultrathin surface SiO_2 layer. Although Si–O–Si moieties make surface non-reactive, they are expected to break upon thermal activation into fragments Si–O + Si, forming thus Si^{3+} point defects that promote the film adherence (see e.g. [44, 45]).

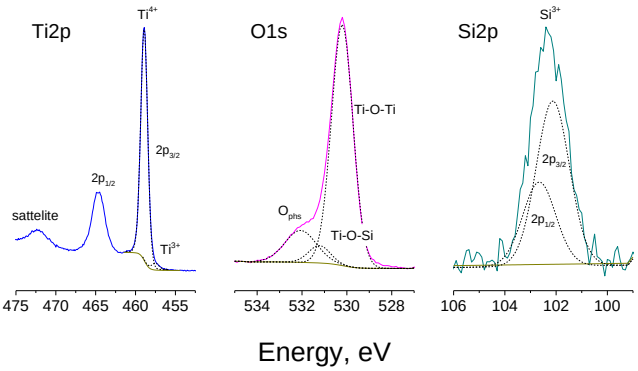

Figure 3: Ti2p, O1s and Si2p XPS spectra of TiO_2 coatings on silica substrates (example of D1coating is given).

Considering the weak Si^{3+} and Ti^{3+} signals assigned to the suboxide cations, one can assume participation of asymmetric (O)3≡Si–Ti≡(O)3 bonds between the titania film and silica substrate. We notice in this connection that annealing at 300 °C promotes the formation of Ti–Si bonds in the Ti/O/Si system with a thin oxidized layer [46] and plasma environment could activate the formation of Ti–Si bonds in our experiments. Furthermore, another solution can be proposed involving formation of (O)3≡Si–O–Ti≡(O)3 bonds. In fact, examination of Ti coordination number changes in $(TiO_2)_x(SiO_2)_{1-x}$ layer has been undertaken by Gaultois and Grosvenor [47], who have shown that Ti2p and Si2p XPS band energies significantly decrease with Ti content increase due to nearest-neighbour and next-nearest-neighbour effects. In particular, the Si2p energy has decreased by 0.74 eV as x increased from 0 to 0.33. Therefore, somewhat large x-value in the interface region could explain the Si2p band position measured in our study. Although we cannot prefer one solution, both (O)3≡Si–Ti≡(O)3 and (O)3≡Si–O–Ti≡(O)3 covalent bonds assure strong adherence of the prepared nanocomposite coatings.

The degradation of cefixime was examined as a model reaction to compare photocatalytic activities of the prepared composite TiO_2 films with different rutile/anatase ratios. The corresponding process followed first order reaction kinetics as shown in Fig. 4. Our experiments showed almost negligible photolytic decomposition of cefixime by UVA light on the timescale of four hours. In contrast, a strong disappearance of pollutant was observed in presence of the photocatalytic coatings. This effect was amplified in D2, D3 and D4 composite coatings containing rutile phase. The photocatalytic rates obtained from the linear fit of the first-order kinetic curves are shown in Fig. 5 as a function of rutile phase content in the anatase-rutile coatings.

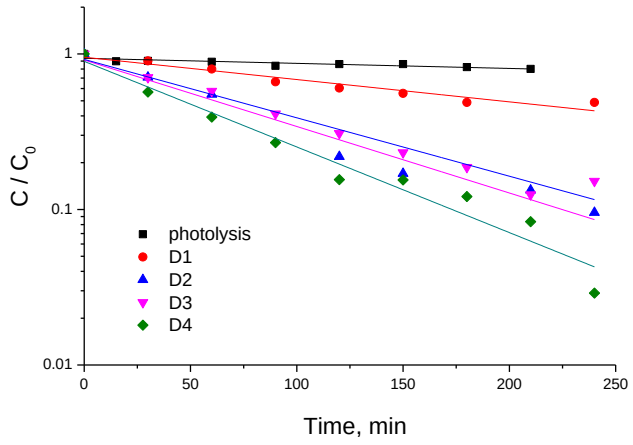

Figure 4: Photocatalytic kinetics of cefixime decomposition in aqueous solutions under UVA (λ=365 nm) light illumination.

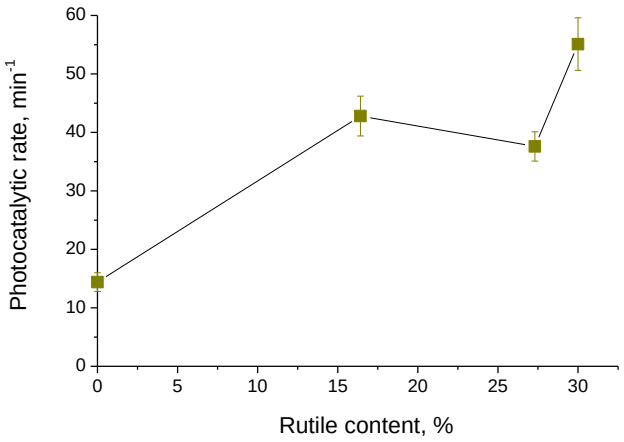

Figure 5: Photocatalytic reaction rate versus rutile content in anatase-rutile nanocoatings with UVA (λ=365 nm) lamp illumination.

These results clearly show the activity enhancement with the increasing content of rutile phase. Furthermore, the activity gain in D2 (16 mol% rutile) compared to pure anatase TiO_2 coating (D1) was 300 %. The following evolution was not so significant, and the overall gain in the best D4 (30 mol% rutile) was about 400 % over D1.

More support to the similar architecture of the prepared films and Degussa P25 TiO_2 nanopowders can be found in TRMC measurements, which reflect the behaviour of photoinduced charges. An important feature of the reference photocatalyst is an intense and long-lasted response of the photoexcited electrons in the conduction band [24]. The TRMC signals of D1 (no O_2) and D2 (2 ml/min O_2) films and Degussa P25 TiO_2 are shown in Fig. 6.

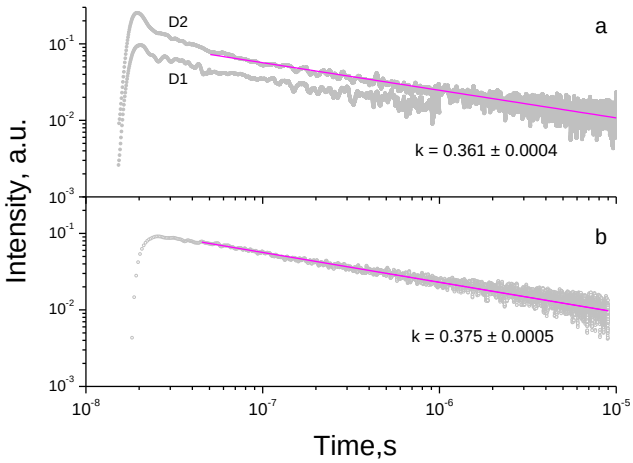

Figure 6: TRMC signals of D1 and D2 coatings (a) and P25 Degussa TiO_2 (b). The power least-squares fits with depicted power constants k are shown by solid lines.

In comparison with D2, the amplitude of D1 coating is 2.7 times lower suggesting a smaller number of long-lived

charges, which is in agreement with its lower photocatalytic activity (Fig. 5). Except for the very beginning related to the photoinduced charges thermalisation, the both curves follow the power-law decay $I=At^{-k}$, which has been previously related to the relaxation of a series of localised states observed via transient absorption spectroscopy [48] and later attributed to the liberation of charges from shallow traps (E_i) of the Urbach tail (E_U) to the conduction band (E_g) with power constant k expressed as $k=k_BT/E_i$ [49], where E_g, E_U and E_i are band gap, Urbach and trap states energies, k_B is Boltzmann constant and T is ambient temperature. According to our measurements, the decay constants of the both materials were very similar and correspond to E_g-$E_i \approx 70$ meV, which is twice larger than E_U at room temperature [50]. The similar amplitudes and decay time of the photoinduced charge kinetics (t>50 ns) suggest a similar energetic structure of the shallow states in both composite anatase-rutile materials. In contrast, evident differences in the thermalisation process kinetics (t<50 ns) was observed between films (Fig. 6a) and nanopowders (Fig. 6b), which understanding requires further studies.

Interesting that the rutile content of the prepared coatings was in the range reported for Degussa P25 TiO_2 nanopowders: 20±10 %. Furthermore, a net gain in the photocatalytic efficiency was observed in presence of rutile, in contrast to the opposite trend reported by Ohtani et al. [10], who has found no synergetic effect of the phases in contact. Further studies concerning photoexcited charges and reaction kinetics by using different pollutant molecules are therefore required in order to confirm the conclusion.

4. Conclusion

The nanocomposite TiO_2 coatings composed of 10-nm crystallinities with anatase/rutile ratio varying between 0 and 30 mol% were prepared on glass substrates via spray-plasma deposition method and controlled via oxygen gas flow in plasma. The coatings formed strong covalent bonds (O)3≡Ti–Si≡(O)3 and (O)3≡Si–O–Ti≡(O)3 with silica substrate, suggesting their strong mechanical adherence. The degradation of cefixime as a model reaction in aqueous solutions under UVA light illumination was examined to compare photocatalytic activities of coatings. We showed that the coatings activity increased with an increase of rutile content by a factor of 3 to 4 compared to pure anatase TiO_2 nanocoatings.

The use of immobilised nanostructured materials in large-scale applications is preferable since permits avoiding (or strongly suppressing) environmental pollution by nanoparticles. The prepared nanocomposite coatings can therefore be an attractive alternative to Degussa P25 powder-like photocatalyst, which rutile content is in the range of that in our materials.

Acknowledgments

Acknowledgments are due to the French Embassy in Tehran for a PhD grant supporting this work.

Declaration

The authors declare no conflict of interest.

References

[1] A. Fujishima, K. Hashimoto, T. Watanabe, TiO_2 photocatalysis: Fundamentals and applications, BKC, Tokyo, 1999.

[2] K. Hashimoto, H. Irie, A. Fujishima, TiO_2 photocatalysis: A historical overview and future prospects. Jap. J. Appl. Phys. **44**, 8269-8285 (2005).

[3] N. Serpone, A. V. Emeline, Semiconductor photocatalysis - past, present, and future outlook. J. Phys. Chem. Lett. **3**, 673-677 (2012).

[4] M. Dell'Edera, C. Lo Porto, I. De Pasquale, F. Petronella, M. L. Curri, A. Agostiano, R. Comparelli, Photocatalytic TiO_2-based coatings for environmental application, Catal. Today **380** 62-83 (2021).

[5] G. Liu, C. Sun, H. G. Yang, S. C. Smith, L. Wang, G. Q. Lu, H-M., Cheng, Nanosized anatase TiO_2 single crystals for enhanced photocatalytic activity. Chem. Commun. **46**, 755-757 (2010).

[6] Q. Sun, Y. Xu, Evaluating intrinsic photocatalytic activities of anatase and rutile TiO_2 for organic degradation in water. J. Phys. Chem. C **114**, 18911-18918 (2010).

[7] A. Y. Ahmed, T. A. Kandiel, T. Oekermann, D. Bahnemann, Photocatalytic activities of different well-defined single crystal TiO_2 surfaces: anatase versus rutile. J. Phys. Chem. Lett. **2**, 2461-2465 (2011).

[8] A. Holm, M. Hamandi, F. Simonet, B. Jouguet, F. Dappozze, C. Guillard, Impact of rutile and anatase phase on the photocatalytic decomposition of lactic acid. Appl. Catal. B **253**, 96-104 (2019).

[9] R. I. Bickley, T. Gonzalez-Carreno, J. S. Lees, L. Palmisano, R. J. D. Tilley, A structural investigation of titanium dioxide photocatalysts. J. Sol. State. Chem. **92**, 178-190 (1991).

[10] B. Ohtani, O. O. Prieto-Mahaney, D. Li, R. Abe, What is Degussa (Evonik) P25? Crystalline composition analysis, reconstruction from isolated pure particles and photocatalytic activity test. J. Photochem. Photobiology A **216**, 179-182 (2010).

[11] D. C. Hurum, A. G. Agrios, K. A. Gray, T. Rajh, M. C. Thurnauer, Explaining the enhanced photocatalytic activity of Degussa P25 mixed-phase TiO_2 using EPR. J. Phys. Chem. B **107**, 4545-4549 (2003).

[12] J. T. Carneiro, T. J. Savenije, J. A. Moulijn, G. Mul, How phase composition influences optoelectronic and photocatalytic properties of TiO_2. J. Phys. Chem. C **115**, 2211-2217 (2011).

[13] J. He, Y. Du, Y. Bai, J. An, X. Cai, Y. Chen, P. Wang, X. Yang, Q. Feng, Facile formation of anatase/rutile TiO_2 nanocomposites with enhanced photocatalytic activity. Molec. **24**, 2996 (2019).

[14] Y. Liu, X. Zou, L. Li, Z. Shen, Y. Cao, Y. Wang, L. Cui, J. Cheng, Y. Wang, X. Li, Engineering of anatase/rutile TiO2 heterophase junction via in-situ phase transformation for enhanced photocatalytic hydrogen evolution. J. Colloid Interf. Sci. **599**, 795-804 (2021).

[15] X. Zhang, J. Chen, S. Jiang, X. Zhang, F. Bi, Y. Yang, Y. Wang, Z. Wang, Enhanced photocatalytic degradation of gaseous toluene and liquidus tetracycline by anatase/rutile titanium dioxide with heterophase junction derived from materials of Institut Lavoisier-125(Ti): Degradation pathway and mechanism studies. J. Colloid Interf. Sci. **588**, 122-137 (2021).

[16] H. D. Jang, S-K. Kim, S-J. Kim, Effect of particle size and phase composition of titanium dioxide nanoparticles on the photocatalytic properties. J. Nanopart. Res. **3**, 141-147 (2001).

[17] J. Marugan, D. Hufschmidt, G. Sagawe, V. Selzer, D. Bahnemann, Optical density and photonic efficiency of silica-supported TiO_2 photocatalysts. Water. Res. **40**, 833-839 (2006).

[18] S. Tieng, K. Chhor, A. Kanaev, New homogeneously doped Fe(III)-TiO_2 photocatalyst for gaseous pollutant degradation. J. Appl. Catal. A **399**, 191-197 (2011).

[19] G. D. Fanou, B. Yao, K. Cheng, O. Brinza, M. Traoré, A. Kanaev, K. Chhor, Elaboration of novel nanoparticulate TiO_2-P25@n-TiO_2 composite for photocatalysis. Int. J. Adv. Appl. Phys. Res. **3**, (2016) 19-25.

[20] K. Baba, C. Lazzaroni, M. Nikravech, Growth of ZnO thin films by spray plasma technique: Correlation between spectroscopic measurements and film properties. Plasma Chem. Plasma Process. **34**, 1433-1446 (2014).

[21] M. Nikravech, Spray plasma device, a new method to process nanostructured layers. Application to deposit ZnO thin layers, J. Nanosci. Nanotechnol. **10**, 1171-1178 (2010).

[22] R. A. Spurr, H. Myers, Quantitative analysis of anatase-rutile mixtures with an x-ray diffractometer. Anal. Chem., **29**, 760-762 (1957).

[23] W.S. Rasband, ImageJ, U. S. National Institutes of Health, Bethesda, Maryland, USA, https://imagej.nih.gov/ij/, 1997-2018.

[24] C. Colbeau-Justin, M. Kunst, D. Huguenin, Structural influence on charge-carrier lifetimes in TiO_2 powders studied by microwave absorption. J. Mat. Sci. **38**, 2429-2437 (2003).

[25] M. Sanchez Mendez, A. Lemarchand, M. Traore, C. Perruchot, C. Sassoye, M. Selmane, M. Nikravech, M. Ben Amar, A. Kanaev, Photocatalytic activity of nanocoatings based on mixed oxide V-TiO_2 nanoparticles with controlled composition and size. Catalysts **11**, 1457 (2021).

[26] Y. Zhao, C. Ji, Y. Wang, X. Liang, J. Fan, Green and efficient degradation of cefixime by 3D flower-like BiOBr: Performance and degradation pathway, Colloids Surf. A **635**, 128024 (2022).

[27] C. J. Howard, T. M. Sabine, F. Dickson Structural and thermal parameters for rutile and anatase. Acta Cryst. B **47**, 462-468 (1991).

[28] H. Zhang, J. F. Banfield, Thermodynamic analysis of phase stability of nanocrystalline titania. J. Mater. Chem. **8**, 2073-2076 (1998).

[29] M. Bouslama, M. C. Amamra, Z. Jia, M. Ben Amar, O. Brinza, K. Chhor, M. Abderrabba**,** J.-L. Vignes, A. Kanaev, New nanoparticulate TiO_2-Al_2O_3 photocatalytic media: Effect of particle size and polymorphism on photocatalytic activity. ACS Catal. **2**, 1884-1892 (2012).

[30] J. Zhang, M. Li, Z. Feng, J. Chen, C. Li, UV Raman spectroscopic study on TiO_2. I. Phase transformation at the surface and in the bulk. J. Phys. Chem. B **110**, 927-935 (2006).

[31] H. Zhang, J. F. Banfield, New kinetic model for the nanocrystalline anatase-to-rutile transformation revealing rate dependence on number of particles. Am. Mineralog. **84**, 528-535 (1999).

[32] R. L. Penn, J. F. Banfield, Formation of rutile nuclei at anatase 112 twin interfaces and the phase transformation mechanism in nanocrystalline titania. Am. Mineralog. **84**, 871-876 (1999).

[33] E. Barborini, I. N. Kholmanov, P. Piseri, C. Ducati, C. E. Bottani, P. Milani, Engineering the nanocrystalline structure of TiO_2 films by aerodynamically filtered cluster deposition. Appl. Phys. Lett. **81**, 3052-3054 (2002).

[34] M. Nikravech, K. Baba, B. Leneindre, F. Rousseau, Role of reactive species in processing materials at laboratory temperature by spray plasma devices. Chem. Papers **66**, 502-510 (2012).

[35] J. Zhang, Q. Xu, M. Li, Z. Feng, C. Li, UV Raman spectroscopic study on TiO_2. II. Effect of nanoparticle size on the outer/inner phase transformations. J. Phys. Chem. C **113**, 1698-1704 (2009).

[36] I. Iatsunskyi, M. Kempinski, G. Nowaczyk, M. Jancelewicz, M. Pavlenko, K. Załeski, S. Jurga, Structural and XPS studies of PSi/TiO_2 nanocomposites prepared by ALD and Ag-assisted chemical etching. Appl. Surf. Sci. **347**, 777-783 (2015).

[37] N. Benito, C. Palacio, Mixed Ti-O-Si oxide films formation by oxidation oftitanium-silicon interfaces. Appl. Surf. Sci. **301**, 436-441 (2014).

[38] N. Zhong, H. Shima, H. Akinaga, Mechanism of the performance improvement of TiO_{2-x}-based field-effect transistor using SiO_2 as gate insulator. AIP Adv. **1**, 032167 (2011).

[39] E-T. Hu, X-X. Liu, Q-Y. Cai, Y. Yao, K-Y. Zang, K-H. Yu, W. Wei, X-X. Xu, Y-X. Zheng, S-Y. Wang, R-J. Zhang, L-Y. Chen, Tunable optical properties of co-sputtered Ti-SiO_2 nanocomposite thin films. Opt. Mater. Express **7**, 2387-2395 (2017).

[40] A. Mehonic, M. Buckwell, L. Montesi, L. Garnett, S. Hudziak, S. Fearn, R. Chater, D. McPhail, A. J. Kenyon, Structural changes and conductance thresholds in metal-free intrinsic SiOx resistive random access memory. J. Appl. Phys. **117**, 124505 (2015).

[41] D. Brassard, D. K. Sarkar, M. A. El Khakani, High-k titanium silicate thin films grown by reactive magnetron sputtering for complementary metal-oxide-semiconductor applications, J. Vac. Sci. Technol. A **22**, 851 (2004).

[42] G. Hollinger, F. J. Himpsel, Probing the transition layer at the SiO_2- Si interface using core level photoemission. Appl. Phys. Lett. **44**, 93-95 (1984).

[43] Ch. Cardinaud, A. Rhounna, G. Turban, B. Grolleau, Analyse XPS des surfaces de Si et SiO_2 exposées aux plasmas de CHF_3 et CHF_3-C_2F_6. Polymérisation et gravure. Rev. Phys. Appl. **24**, 309-321 (1989).

[44] J. T. Yates, Water interactions with silica surfaces: A big role for surface structure. Surf. Sci. **565**, 103-106 (2004).

[45] S. Wendt, M. Frerichs, T. Wei, M.S. Chen, V. Kempter, D.W. Goodman, The interaction of water with silica thin films grown on Mo(112). Surf. Sci. **565**, 107-120 (2004).

[46] R. Butz, G. W. Rubloff, P. S. Ho, Chemical bonding and reactions at Ti/Si and Ti/oxygen/Si interfaces. J. Vac. Sci. Technol. A **1**, 771-775 (1983).

[47] M. W. Gaultois, A. P. Grosvenor, XANES and XPS investigations of $(TiO_2)_x(SiO_2)_{1-x}$: the contribution of final-state relaxation to shifts in absorption and binding energies. J. Mater. Chem. **21**, 1829-1836 (2011).

[48] A. C. Sobennikov, S. A. Antipin, F. E. Gostev, O. M. Sarkisov, V. A. Nadtochenko, Yu. E. Lozovik, Femtosecond relaxation dynamics of photoinduced nanocrystalits TiO_2 in aqua suspensions. Khim. Fiz. **24**, 9-13 (2005) (in Russian).

[49] K. Cheng, K. Chhor, J.-P. Passarello, C. Colbeau-Justin, A. Kanaev, Photocatalytic nanoparticulate $Zr_xTi_{1-x}O_2$ coatings with controlled homogeneity of elemental composition. Chem. Select **3**, 11118-11126 (2018).

[50] H. Tang, F. Levy, H. Berger, P. E. Schmid, Urbach tail of anatase TiO_2. Phys. Rev. B **52**, 7771-7774 (1995).